



**HAL**  
open science

# Physical characteristics and dynamics of the coastal Latex09 Eddy derived from in situ data and numerical modeling.

Marion Kersale, Anne Petrenko, Andrea M. Doglioli, I. Dekeyser, Francesco  
Nencioli

► **To cite this version:**

Marion Kersale, Anne Petrenko, Andrea M. Doglioli, I. Dekeyser, Francesco Nencioli. Physical characteristics and dynamics of the coastal Latex09 Eddy derived from in situ data and numerical modeling.. *Journal of Geophysical Research. Oceans*, 2013, 118, pp.399-409. 10.1029/2012JC008229 . hal-00756955

**HAL Id: hal-00756955**

**<https://hal.science/hal-00756955>**

Submitted on 24 Nov 2012

**HAL** is a multi-disciplinary open access archive for the deposit and dissemination of scientific research documents, whether they are published or not. The documents may come from teaching and research institutions in France or abroad, or from public or private research centers.

L'archive ouverte pluridisciplinaire **HAL**, est destinée au dépôt et à la diffusion de documents scientifiques de niveau recherche, publiés ou non, émanant des établissements d'enseignement et de recherche français ou étrangers, des laboratoires publics ou privés.

**1 Physical characteristics and dynamics of the coastal**  
**2 Latex09 Eddy derived from *in situ* data and**  
**3 numerical modeling.**

M. Kersalé,<sup>1</sup> A. A. Petrenko,<sup>1</sup> A. M. Doglioli,<sup>1</sup> I. Dekeyser,<sup>1</sup> F. Nencioli<sup>1</sup>

---

<sup>1</sup>Aix-Marseille Université, Université du  
Sud Toulon-Var, CNRS/INSU, IRD, MIO,  
UM 110, 13288, Marseille, Cedex 09, France.

**Abstract.**

We investigate the dynamics of a coastal anticyclonic eddy in the western part of the Gulf of Lion (GoL) in the northwestern Mediterranean Sea during the Latex campaign in the summer 2009 (Latex09). The sampling strategy combines SST satellite imagery, hull-mounted ADCP data, CTD casts and drifter trajectories. Our measurements reveal an anticyclonic eddy (*Latex09 eddy*) with a diameter of  $\sim 23$  km and maximum depth of 31 m, centered at  $3^{\circ}34'E - 42^{\circ}33'N$ . We use a high resolution, 3-dimensional, primitive equation numerical model to investigate its generation process and evolution. The model is able to reproduce the observed eddy, in particular its size and position. The model results suggest that the *Latex09 eddy* is induced by a large anticyclonic circulation in the northwestern part of the GoL, pushed and squeezed toward the coast by a meander of the Northern Current. This represents a new generation mechanism that has not been reported before. The post generation dynamics of the eddy is also captured by the model. The collision of the *Latex09 eddy* with Cape Creus results in a transient structure, which is depicted by the trajectories of two Lagrangian drifters during Latex09. The transient structure and its advection lead to a transfer of mass and vorticity from the GoL to the Catalan shelf, indicating the importance of mesoscale structures in modulating such exchanges in the region.

*Keywords:* Coastal eddies, *in situ* measurements, numerical modeling, mesoscale, Gulf of Lion.

## 1. Introduction

26 Continental shelf processes are often affected by large eddies approaching the continental  
27 slope from the deep ocean. In several open-ocean studies these energetic features of the  
28 ocean circulation have been observed and described during their propagation onto the  
29 continental shelf [Lewis and Kirwan Jr., 1985; Kirwan Jr. et al., 1988; Vukovich and  
30 Waddel, 1991; Vidal et al., 1992; Richardson et al., 1994; Fratantoni et al., 1995; Hamilton  
31 et al., 1999]. Studies that focus specifically on coastal eddies (the ones developed on the  
32 continental shelf) are much scarcer.

33 *Mitchelson-Jacob and Sundby* [2001] have observed coastal eddies through the analysis  
34 of satellite images on the continental shelf of Norway. They found that the size of these  
35 eddies depends on the width of the fjord, with a diameter between 20 km to 60 km. An  
36 anticyclonic eddy was sampled during a field campaign and followed by numerous drifters  
37 [*Mitchelson-Jacob and Sundby*, 2001; *Saetre*, 1999]. This anticyclonic eddy appeared to  
38 be a quasi-stationary feature [*Eide*, 1979], reaching 140 m depth. The wind direction, the  
39 depth of the near-surface layer and the presence of stratification have been identified as  
40 strong factors influencing the characteristics of these eddies. The strong currents in this  
41 region have been linked directly to the formation of these eddies.

42 Mesoscale anticyclonic eddies have been also investigated inside the Gulf of Alaska.  
43 These eddies are named according to the location of their generation: *Sitka Eddies*  
44 [*Tabata*, 1982], *Haida Eddies* [*Crawford and Whitney*, 1999] and *Yakutat Eddies* [*Ladd*  
45 *et al.*, 2005]. They are baroclinic structures with a diameter of 150-300 km. These eddies  
46 generally form in winter and detach from the continental margin in late winter and spring.

47 *Haida Eddies* usually form in the outflow of coastal waters [*Crawford, 2002; Di Lorenzo*  
48 *et al., 2005*]. *Sitka* and *Yakutat Eddies* are believed to form in flow instabilities along the  
49 continental slope [*Melson et al., 1999*].

50 Coastal cyclonic eddies have been also investigated further south along the British  
51 Columbia shelf. The presence of a quasi-stationary eddy, the *Juan de Fuca Eddy*, on  
52 the southern Vancouver Island shelf has been described in several studies [*Tully, 1942;*  
53 *Freeland and Denman, 1982; Denman and Freeland, 1985; Freeland and McIntosh, 1989;*  
54 *MacFadyen et al., 2008*]. This eddy is a topographically confined eddy which develops off  
55 Cape Flattery in spring with a diameter of 80 km below 100 m depth.

56 Current separation from capes has been proposed as an explanation for eddy formation  
57 in many coastal flows behind capes or headlands [*Signell and Geyer, 1991; Doglioli et al.,*  
58 *2004; Magaldi et al., 2010*]. However, in the case of the buoyant flow around Cape Flattery,  
59 the Coriolis force does not tend to maintain the current close to the coast [*MacFadyen and*  
60 *Hickey, 2010*]. In fact, the eddy generation has been linked to two upwelling processes  
61 occurring in the area with the important contribution of tidal forcing in the initial eddy  
62 generation process [*Foreman et al., 2008; MacFadyen and Hickey, 2010*].

63 In general, the dynamics and the role of mesoscale coastal eddies are very complex  
64 and different from one region to another. These eddies can translate away from their  
65 generation region with the mean flow [*Crawford et al., 2007; Mitchelson-Jacob and Sundby,*  
66 *2001*] or they can be quasi-stationary and linked to the topography [*Eide, 1979; Freeland*  
67 *and Denman, 1982*]. Other studies highlight the role of mesoscale eddies on coastal  
68 upwelling processes in idealized ecosystems [*Lathuilière et al., 2010*] or in the Ligurian Sea  
69 [*Casella et al., 2011*]. In either case, they have profound impacts on local mechanisms

70 of water transport, vertical mixing and circulation processes. They are often biologically  
71 rich regions because they can transport nutrient-rich coastal water off the coast to open  
72 ocean.

73 The Gulf of Lion (GoL) is particularly relevant for the study of coastal mesoscale struc-  
74 tures. The GoL is located in the northwestern Mediterranean Sea and is characterized by  
75 a large continental margin (Figure 1). Its hydrodynamics is complex and highly variable  
76 [Millot, 1990]. The circulation is strongly influenced by the Northern Current (NC), which  
77 constitutes an effective dynamical barrier blocking coastal waters on the continental shelf  
78 [Albérola *et al.*, 1995; Sammari *et al.*, 1995; Petrenko, 2003]. Exchanges between the GoL  
79 and offshore waters are mainly induced by processes associated with the NC [Conan and  
80 Millot, 1995; Flexas *et al.*, 2002; Petrenko *et al.*, 2005].

81 In the eastern part of the GoL, south of Marseilles, Allou *et al.* [2010] have observed the  
82 presence of anticyclonic eddies between the NC and the coast using current meter data and  
83 surface currents measured by High Frequency (HF) radars. The eddies are of diameters  
84 12 to 28 km and they are coherent down to a depth of 140 m. Baroclinic instability of the  
85 NC is a possible generation mechanism [Flexas *et al.*, 2002]. Schaeffer *et al.* [2011] have  
86 also observed anticyclonic eddies, with a diameter of 20-40 km, in the eastern part of the  
87 GoL with HF radars and numerical simulations. They have shown that their generation  
88 mechanism is related to the local wind conditions. After their generation, some of the  
89 eddies are advected by the NC towards the western part of the shelf.

90 The instability of the NC and its role on the advection of eddies has been also proposed  
91 to explain the presence of anticyclonic eddies on the Catalan continental shelf [Rubio *et al.*,  
92 2005]. However Rubio *et al.* [2009a] rejected their previous hypothesis and suggested that

93 the process of flow separation due to a topographic barrier generates these eddies. A  
94 possible mechanism for the generation of the Catalan eddies is described by *Garreau*  
95 *et al.* [2011] in terms of release of potential energy from other eddies located in the GoL.

96 Through ADCP measurements and numerical simulations *Estournel et al.* [2003] showed  
97 a large anticyclonic circulation located in the northwestern part of the GoL. In this part  
98 of the GoL, a mesoscale anticyclonic circulation was first described by *Millot* [1979, 1982].  
99 *Hu et al.* [2009, 2011a] showed the presence of a mesoscale eddy by a combined use of  
100 data from satellite observations, *in situ* measurements and numerical modeling. The  
101 eddies were baroclinic structures extending throughout the mixed layer (30 to 50 m),  
102 often elliptical in shape and about 20-30 km in diameter (elliptical diameter is defined as  
103 the mean of the minor and major axes). The generation process of the eddies mentioned  
104 by *Hu et al.* [2009, 2011a] required two conditions: a persistent and strong northwest wind  
105 and a strong stratification [*Hu et al.*, 2011b].

106 The LAgrangian Transport EXperiment (LATEX) project (2008-2011) is designed to  
107 study the mechanisms of formation of anticyclonic eddies and their influence on cross-shelf  
108 exchanges in the western part of the GoL. The dynamics of mesoscale eddies is particularly  
109 important in this part of the GoL since it represents a key region for regulating the outflow  
110 from the continental shelf [*Hu et al.*, 2011a; *Nencioli et al.*, 2011].

111 The aim of the present study is to analyze the dynamical characteristics and generation  
112 processes of such eddies during the summer of 2009. The methods used are described in  
113 Section 2. Results based on a combination of satellite and *in situ* oceanographic data,  
114 as well as numerical results are presented in Section 3. The general characteristics of the

115 observed eddies, their possible generation mechanisms and their behaviors are discussed  
116 in Section 4.

## 2. Methods

117 The LATEX strategy was based on a combined use of Eulerian and Lagrangian *in situ*  
118 measurements, satellite data and numerical modeling. The Latex09 campaign, conducted  
119 from August 24 to 28, 2009 on board the R/V Téthys II, was the second field experiment  
120 of the LATEX project.

### 2.1. Data

121 Identifying the center of an eddy is one of the greatest challenges in the eddy commu-  
122 nity. To characterize the observed eddy, this field campaign took advantage of various  
123 observational data.

124 The data collected during Latex09 came from satellite, ship-based and drifter obser-  
125 vations. Satellite data include SeaWiFs chlorophyll concentration [ $\text{mg m}^{-3}$ ] from the  
126 NASA's Goddard Space Flight Center (GSFC) and Sea Surface brilliance Temperature  
127 provided by Météo-France (referred to as  $SST_b$ ). During the campaign, the data were  
128 sent to the R/V Téthys II to help tracking the mesoscale features in near real-time.

129 A VMBB-150 kHz ship-based Acoustic Doppler Current Profiler (ADCP) was used to  
130 measure current velocities (Figure 2). Following *Petrenko et al.* [2005], the instrument was  
131 configured for recording 1 minute ensemble averages, providing horizontal currents with  
132 a vertical resolution of 4 m from 11 to 247 m of depth. The software for ADCP raw data  
133 treatment is provided by the French Institut National des Sciences de l'Univers (INSU -  
134 CNRS) technical division. At each depth, the ADCP horizontal currents can be analyzed

135 in near real-time during the entire campaign using the method described by *Nencioli*  
136 *et al.* [2008]. A searching grid of  $30\times 30$  points corresponding to a  $30\times 30$  km square area  
137 was imposed within each transect. Each grid point was tested as a possible location,  
138 at that depth, for the center of the eddy. For each grid point, the components of the  
139 ADCP velocities from a transect were decomposed into radial and tangential components  
140 with respect to the reference frame centered at each point. The center, hereafter referred  
141 to as single-depth transect center, was estimated as the grid point for which the mean  
142 tangential velocity computed from the nearest ADCP records (black vectors - Figure 2)  
143 was maximum.

144 In the present paper, the analysis focuses on Transect 1 and three other transects that  
145 cross its center (Figure 2). Transect 2 is orthogonal to the coast (Figure 2b), Transect 3  
146 is orthogonal to the continental slope (Figure 2c) and Transect 4 follows it (Figure 2d).  
147 The start and end times for each transect are reported in Table 1.

148 During the transect mapping, we also collected a total of 25 profiles at specific locations  
149 using a SeaBird SBE 19 CTD. We only show three of the CTD profiles, one inside the  
150 eddy (CTD\_in, blue cross - Figure 5a), one at the edge (CTD\_edge, red cross) and one  
151 outside the eddy (CTD\_out, black cross), representing eddy center, eddy edge and outside  
152 conditions, respectively. Two satellite-tracked drifters, anchored at 15 m depth, were  
153 deployed within the eddy to track the fluid motion. Drifter positions were provided by  
154 the Argos system in quasi-real time. In addition, sea surface temperature, salinity and  
155 fluorescence were measured continuously at the surface by the ship's thermosalinometer  
156 SBE 21.

## 2.2. Ocean model

157 In addition to the *in situ* measurements, the eddy dynamics have been investigated using  
158 Symphonie, a 3-dimensional, primitive equation model, with a free sea surface, hybrid  
159 sigma coordinates, based on Boussinesq and hydrostatic approximations [*Marsaleix et al.*,  
160 2006, 2008]. We use the upwind-type advection-diffusion scheme adapted by *Hu et al.*  
161 [2009] to improve the ability of the model to reproduce coastal mesoscale eddies in the  
162 western part of the GoL. In the present study, the model is implemented over the whole  
163 GoL with an horizontal resolution of  $1 \text{ km} \times 1 \text{ km}$  (Figure 1). The vertical discretization  
164 consists of 40-hybrid vertical levels. The vertical resolution varies from 1 m in the upper  
165 ocean to 40 m near the bottom.

166 This high resolution model is one-way nested to a coarse grid model ( $3 \text{ km} \times 3 \text{ km}$ )  
167 covering a larger domain. The initial and open boundary conditions for the larger domain  
168 are provided by the Mediterranean Forecasting System (MFS) general circulation model  
169 [*Pinardi*, 2003] with a resolution of  $1/8^\circ$ . The atmospheric forcing is obtained from the  
170 3-hr outputs of the meteorological model Aladin of Météo-France with a spatial resolution  
171 of  $0.1^\circ \times 0.1^\circ$ . The daily fresh water fluxes from the major rivers are taken into account.  
172 The readers are referred to *Hu et al.* [2011b] for more details about the model settings.

173 This model was run from 2001 to 2008 and the results were analyzed by *Hu et al.*  
174 [2011b]. In the present study it is run for 2009, with a restart from the previous simulation.  
175 The daily outputs of current velocity components, salinity, temperature and density are  
176 averaged over 24 hours of simulation, to filter out the diurnal cycle. We have verified that  
177 the 24-hours average is also effective in filtering out the inertial oscillations, that is of

178 ~17.5 hours in the GoL. The remaining unfiltered inertial kinetic energy represents 1-5%  
179 of the total average kinetic energy.

180 In order to study the generation process with the same criteria used in the study of *Hu*  
181 *et al.* [2011a], we consider the wind as a strong and persistent northwesterly wind event  
182 when its amplitude is larger than, or equal to,  $8 \text{ m s}^{-1}$ , and its direction is between  $270^\circ$   
183 and  $360^\circ$  for at least 75% of the time during the last three days. In order to investigate  
184 the variation of stratification, the potential energy anomaly  $\phi$  is chosen as the indicator of  
185 the stability of the water column [*Hu et al.*, 2011a; *Burchard and Burchard*, 2008; *De Boer*  
186 *et al.*, 2008]. The value of  $\phi$  decreases with the level of homogeneity through the water  
187 column. Values of  $\phi$  reaching  $20 \text{ J m}^{-3}$  ( $100 \text{ J m}^{-3}$ ) indicate a weak (strong) stratification.  
188 An intermediate stratification is defined with a value  $\phi$  around  $60 \text{ J m}^{-3}$ .

189 The utility program WATERS [*Doglioli et al.*, 2007] is used to objectively identify and  
190 follow the coherent eddy structures in our numerical simulations. This automatic detec-  
191 tion of 3-dimensional eddy structures was first conducted with a high-resolution numerical  
192 model of the oceanic region around South Africa [*Doglioli et al.*, 2007]. More recently,  
193 WATERS has been used by *Rubio et al.* [2009b] to investigate mesoscale activity in the  
194 Benguela upwelling system and by *Dencausse et al.* [2010] to study the routes of Agulhas  
195 rings. In the South Atlantic Ocean, *Souza et al.* [2011] also tested the performances of  
196 WATERS in comparison with other automatic identification algorithms for the quantifi-  
197 cation and characterization of mesoscale eddies. In coastal waters, *Hu et al.* [2009, 2011b]  
198 successfully used WATERS to identify anticyclonic eddies in the GoL. The method is  
199 based on wavelet analysis of horizontal slices of modeled relative vorticity to extract co-  
200 herent structures, providing a set of grid points and a center associated to each eddy. The

center of the modeled eddy is defined as the maximum in magnitude of relative vorticity. For each eddy, tracking can be performed both backward and forward in time to find the “birth” and the “death” of the eddy. At each time step, the eddy’s diameter,  $D$ , is defined as the average between the zonal ( $D^{EW}$ ) and the meridional ( $D^{NS}$ ) cords that intercept each eddy center with both endpoints on the edge of the structure. This definition accounts for stretched shapes. The analysis is repeated at each depth level ( $k$ ) to diagnose the vertical extent of the identified eddy. The vertical tracking ends at the level number ( $i_z$ ) before the eddy signal in relative vorticity becomes too weak to be detected. With this method the reference diameter can be calculated as :

$$D = \frac{1}{i_z} \sum_{k=1}^{i_z} \frac{D_k^{EW} + D_k^{NS}}{2} \quad (1)$$

For stretched eddies, the variance made on the calculation of  $D$  with eq(1) is estimated as:

$$D_{var} = \frac{1}{i_z} \sum_{k=1}^{i_z} \left( \frac{D_k^{EW} + D_k^{NS}}{2} - D \right)^2 \quad (2)$$

In the following, our results are written as  $D \pm \sqrt{D_{var}}$ .

### 3. Results

#### 3.1. *In situ* experiment

An eddy was detected before the campaign from the analysis of the  $SST_b$  and SeaWiFs chlorophyll-a surface concentration. On August 20, lower  $SST_b$  ( $\Delta SST_b = 1.5^\circ\text{C}$ ) and lower chlorophyll-a concentration ( $\Delta Chl_a = 0.4 \text{ mg m}^{-3}$ ) within the eddy relative to the surroundings, allowed for its identification. The eddy’s center position was estimated to be  $3^\circ 30' \text{E} - 42^\circ 36' \text{N}$ . At the beginning of the campaign, during Transect 1, we crossed the whole eddy, passing through its satellite eddy center.

221 On the basis of ADCP velocities, the single-depth transect center for Transect 1 at 15 m  
222 depth *C1\_15* was estimated to be at 3°33'E - 42°33'N (black cross - Figure 2a). Succes-  
223 sively, we conducted a systematic mapping of the eddy by performing several transects  
224 passing through that position.

225 ADCP horizontal current velocity vectors at 15 m depth reveal a clockwise circulation  
226 associated with an anticyclonic eddy (Figure 2). We also detect a strong current with  
227 a southwestward direction at the southeastern part of the eddy, corresponding to the  
228 presence of the NC (Figures 2b,c).

229 Tangential velocity at 15 m depth and surface temperature measured during Transect  
230 3 are shown in Figure 3 with respect to the distance from the single-depth transect center  
231 for Transect 3 at 15 m depth (*C3\_15* - black cross - Figure 2c). Since Transect 3 did not  
232 pass directly through *C3\_15*, the data are measured only up to a distance of 1.4 km from  
233 it. At this distance, the values of tangential velocities are not zero but close to zero. Then  
234 they increase linearly with radial distance to reach maximum values of about  $0.4 \text{ m s}^{-1}$   
235 at roughly 9 km (15 km) for the northwestern (southeastern) part of the transect. These  
236 values show that the eddy is not symmetric. After reaching the maximum values, the  
237 tangential velocities slowly decrease as the radial distance further increases. The portion  
238 of the eddy characterized by a constant angular velocity corresponds to the portion of the  
239 eddy that rotates as a solid body (dashed line - Figure 3a). Thus the distance between  
240 the two maximum values of tangential velocities at the edges of the eddy, evaluated to be  
241  $\sim 24 \text{ km}$  (9 km +15 km), represents the diameter of the solid body rotation of the eddy.

242 The distribution of surface temperature from the thermosalinometer, with respect to  
243 radial distance from *C3\_15*, shows warmer waters at the southeastern border of the eddy

244 (Figure 3b). The plot shows the presence of a strong temperature gradient (more than  
245  $1^{\circ}\text{C}$  over a distance of  $\sim 3$  km). This sudden temperature increase is located at 15 km  
246 from *C3\_15*, and coincides with the maximum value of tangential velocity component, and  
247 hence the edge of the solid-body part of the eddy.

248 The vertical section of tangential velocity in Figure 4a, between 11 and 19 m depth,  
249 shows a typical eddy structure with two lobes of relatively high positive tangential ve-  
250 locities that extend on the two sides of the axis. A common feature for the tangential  
251 velocities at these depths is a quite rapid increase from the single-depth transect center  
252 for Transect 3 up to a distance of 10-15 km where they reach their maximum values.  
253 Between 19 and 31 m depth, tangential velocities never reach near zero values close to the  
254 single-depth transect center for Transect 3, as those at shallower depths do. This occurs  
255 because the deeper positions of the single-depth transect centers for Transect 3 tend to be  
256 further away from the transect (Figure 4b), indicating that the axis of the eddy is tilted.  
257 Below 31 m depth, velocities decay relatively rapidly with depth, so that the anticyclonic  
258 circulation associated with the eddy is limited to the upper 31 m. At deeper depths,  
259 the presence of the NC is most distinguishable between  $3^{\circ}42'\text{E}$  and  $3^{\circ}46'\text{E}$  with velocities  
260 around  $0.2\text{ m s}^{-1}$ . The impact of the NC on the anticyclonic eddy is also obvious from  
261 the higher tangential velocities on its southeastern part at the surface.

262 In the preceding section we have only presented the analysis of Transect 3 at 15 m  
263 depth, since similar evaluations made for all the other transects gave similar results.  
264 Tangential velocities with respect to radial distance from the single-depth transect center  
265 have been analyzed for all the transects at three depths (11 m, 15 m, 19 m). These  
266 depths have been chosen because they are the shallowest bins available from the ADCP

267 and are within the studied eddy. The resulting estimations of the diameter and the  
268 position of the single-depth transect centers are summarized in Table 2. In the table we  
269 introduce two other center estimates. The depth-averaged transect centers are defined  
270 as the mean of the positions of the single-depth transect centers. The transect-averaged  
271 eddy center, hereafter named for simplification eddy center  $\mathbf{C}$ , is defined as the mean of  
272 the positions of the depth-averaged transect centers. The estimated position of the eddy  
273 center corresponds to the depth-averaged transect center for Transect 1 (C1-Table 2).

274 Transects 3 and 4 are approximately meridional and zonal, respectively, and thus they  
275 are also roughly perpendicular (Figure 2). Therefore, in order to estimate the diameter  
276 from *in situ* data, we apply eq(1) where  $D_{EW}$  ( $D_{NS}$ ) is the distance between the two  
277 maximum values of tangential velocities on Transect 3 (4) at the three reference depths  
278 (11 m, 15 m, 19 m). The diameter of the eddy is thereby estimated to be  $22.7 \pm 1.2$  km.

279 Another way to evaluate the vertical extension of the eddy comes from the analysis of the  
280 vertical profiles of temperature and fluorescence (Figure 5). The temperature profiles show  
281 values between  $23.0^{\circ}\text{C}$  and  $23.6^{\circ}\text{C}$  at the surface and a progressive decrease with depth  
282 to a value of  $13.4^{\circ}\text{C}$  at about 150 m depth (Figure 5b). A strong thermocline is observed  
283 between 8 and 18 m (20 and 35 m), at station CTD\_out (CTD\_in), outside (inside) the  
284 eddy. Indeed the anticyclonic eddy corresponds to a deepening of the thermocline. We  
285 also notice a weak value of fluorescence at the surface for all three profiles (Figure 5c). A  
286 fluorescence peak reaching  $2.5 \mu\text{g l}^{-1}$  is visible at 50 m depth outside the eddy (station  
287 CTD\_out); it decreases to less than  $2 \mu\text{g l}^{-1}$  at the edge of the eddy (station CTD\_edge).  
288 Only a faint maximum of  $0.6 \mu\text{g l}^{-1}$  can be found at 70 m depth inside the eddy (station

CTD\_in), deeper than the thermocline. This agrees with a reduced phytoplankton biomass induced by the downwelling associated with anticyclonic eddies [Siegel *et al.*, 2011].

### 3.2. Modeling results

The study of the numerical model outputs with the wavelet analysis allows us to retrieve information about the various mesoscale structures in the study area in 2009. Hereafter, we adopt the terminology introduced by *Hu et al.* [2011b] who defined “long-life” eddies as the ones which last for at least 15 days. We have thoroughly studied year 2009 and two modeled “long-life” anticyclonic eddies are identified. The wavelet analysis shows that the first “long-life” eddy (hereafter *A1*) is generated on June 28 and lasts until July 20, while the second eddy is generated on August 16 and lasts until October 12. The latter is considered to be analogous to the eddy sampled during *Latex09* and described in Section 3.1, and hence is hereafter referred to as *A2-Latex09*.

First, we want to understand the generation mechanism of these two eddies. The generation process of eddy *A1* starts with a strong northwesterly wind observed from June 19 to 21. This strong wind, with an amplitude equal to  $18 \text{ m s}^{-1}$ , induces an Ekman transport piling the water close to Cape Creus. Then a northward current along the Roussillon coast starts on June 26. The closing of this Ekman southwestward drift and coastal current jet generates the anticyclonic eddy. An intermediate stratification has also been identified with an absolute value of potential energy anomaly more than  $60 \text{ J m}^{-3}$ . These facts indicate that the generation process of the eddy *A1* corresponds to the one described by *Hu et al.* [2011b] for all “long-life” eddies between 2001 and 2008.

On the other hand, the generation process of the second eddy, *A2-Latex09*, is different. During a weak wind event (Figure 6a), we first observe the generation of a large-scale

311 anticyclonic circulation extending to all the western GoL on July 20 (Figure 6e). In  
312 the western part of the GoL, the positive sea surface height (Figure 6f) corresponds  
313 to an anticyclonic circulation extending south of Cape Creus. A meander of the NC  
314 approaches this large anticyclonic circulation, squeezing it and reinforcing the current at  
315 its southeastern edge. This occurs during a northwesterly wind event (Figure 6b) that  
316 started on August 6. It produces a localized upwelling south of Cape d'Agde but smaller  
317 than the one observed in the generation process proposed by *Hu et al.* [2011b]. During  
318 this generation process, the wind can be classified on August 27 as a strong northwesterly  
319 wind event ( $16 \text{ m s}^{-1}$ ) but not persistent since its occurrence during the last three days  
320 is less than 75%. A strong stratification has also been identified with an absolute value  
321 of potential energy anomaly more than  $100 \text{ J m}^{-3}$ . On August 16 the wavelet analysis  
322 identifies two anticyclonic eddies corresponding to the zonal separation of the anticyclonic  
323 area in two smaller areas (Figure 6g). Indeed the NC meander seems to push and squeeze  
324 the structure to the west. Then, as the presence of the coast blocks its progression, the  
325 structure becomes separated in two structures: one eddy on the shelf of the GoL (*A2-*  
326 *Latex09*) and one moving inside the Catalan Basin. On August 27, these structures are  
327 clearly distinct (Figure 6h). In the following, the eddy in the Catalan shelf is referred to  
328 as the *Catalan Eddy*.

329 In the next paragraphs, the characteristics of *A2-Latex09* on August 27 are presented  
330 for comparison with the *in-situ* data sampled at the same time (Table 1). The modeled  
331 *A2-Latex09* extends throughout the mixed layer until 37 m depth. The wavelet analysis  
332 identifies an eddy centered at  $3^{\circ}26'E-42^{\circ}36'N$  with a diameter of  $28.6 \pm 1.4 \text{ km}$ . The  
333 position of the eddy's center is calculated as the mean of its positions between 1 and 37 m

334 depth with a vertical step of 4 m. This vertical step is chosen to be equal to the vertical  
335 resolution of the ADCP for a better comparison. The diameter of the eddy is obtained  
336 applying eq(1) and (2) to North/South and East/West transects across the modeled eddy  
337 with the same vertical resolution between the same depth interval.

338 Moreover the model has been also useful to examine the post generation mechanism of  
339 *A2-Latex09*. Indeed on August 31, *A2-Latex09* encounters Cape Creus. Following this  
340 event, a transient anticyclonic structure is generated downstream the cape on September  
341 3, detaching from *A2-Latex09*. A 3D view of potential vorticity (Figure 7) in the domain  
342 gives a good visualization of the phenomenon. In order to quantify the transfer, a balance  
343 of mass has been computed from the model results between August 30 and September 3.

344 The transient structure represents  $\sim 33\%$  of the *A2-Latex09*'s mass. The loss of mass of  
345 the eddy *A2-Latex09* is estimated to be  $\sim 41\%$ . As a result, 8% of the mass is dispersed  
346 during this separation. The gain expected on the mass of the *Catalan Eddy* can not be  
347 estimated properly since the latter is too close to the model domain boundary.

348 A 2D view of the relative vorticity (Figure 8a) shows the presence of the transient an-  
349 ticyclonic structure between *A2-Latex09* and the *Catalan Eddy*. The dynamics simulated  
350 by the model is supported by the trajectories of two Lagrangian drifters, released during  
351 the Latex09 campaign, from August 26 to September 12 (Figure 8b). On August 26,  
352 drifter No. 83631 (blue line) was deployed near the eddy center **C** and drifter No. 83632  
353 (purple line) near the western outer edge of the eddy. Drifter No. 83631 made one full  
354 loop around the eddy in 81 hours. Its trajectory stopped looping around the eddy on  
355 September 2 and then drifted northward. Drifter No. 83632 started to loop around the  
356 eddy but, on August 30, it began to drift southward moving away from it. Checking the

357 rotation period of this buoy to ascertain the nature of this feature, we found a rotation pe-  
 358 riod of 39 hours, corresponding approximately to half the rotation period of *A2-Latex09*.  
 359 This rotation does not correspond to an inertial oscillation, which has a typical period of  
 360  $\sim 17.5$  hours in the GoL. This fact confirms the hypothesis that the drifter is trapped in  
 361 the transient structure. On September 6, Drifter No. 83632 got trapped in the *Catalan*  
 362 *Eddy* located at  $3^{\circ}11'E-41^{\circ}35'N$ .

#### 4. Discussion and Concluding remarks

363 The generation and characteristics of a coastal anticyclonic eddy detected in the western  
 364 part of the GoL have been studied from a combination of *in situ* measurements and  
 365 numerical modeling from the end of August 2009 to the middle of October 2009.

366 On the basis of *in situ* measurements, the anticyclonic eddy is centered at  $3^{\circ}34'E-$   
 367  $42^{\circ}33'N$  and is characterized by a diameter of  $22.7 \pm 1.2$  km, reaching a maximal depth of  
 368 31 m. The observed anticyclonic eddy is well reproduced by the model as shown by the  
 369 numerical relative vorticity field on September 3 (Figure 8a). The major characteristics  
 370 of this modeled eddy agree with the observations, although its horizontal dimensions are  
 371 slightly larger than the observed ones. The diameter of the simulated eddy is  $28.6 \pm 1.4$  km.  
 372 This eddy is approximately situated at the same location as the measured one, slightly  
 373 more northwestward ( $3^{\circ}26'E-42^{\circ}36'N$ ).

374 To characterize the dynamics of the eddy, we computed the local Rossby number ( $R_o =$   
 375  $\frac{V_{max}}{R_{max}f}$ ) and the the Rossby radius of deformation ( $R_d = \frac{\sqrt{g'H'}}{f}$ ).  $V_{max}$  is calculated as the  
 376 mean of the maximum tangential velocities on Transects 3 and 4 at the three reference  
 377 depths.  $R_{max}$  is calculated as half of the reference diameter  $D$ , defined in eq(1). With  
 378  $V_{max}$  equal to  $0.35 \text{ m s}^{-1}$  and  $R_{max}$  about 13.5 km, the resulting local Rossby number of

379 the eddy is 0.26. To compute  $R_d$ , the reduced gravity was calculated as  $g' = \frac{\rho_2 - \rho_1}{\rho_2} g$ , with  
 380  $\rho_2 = 1029.04 \text{ kg m}^{-3}$ , the mean density below the mixed layer, and  $\rho_1 = 1025.75 \text{ kg m}^{-3}$ ,  
 381 the mean density within the mixed layer. The mixed layer depth was 10.9 m. The resulting  
 382  $R_d$  is 5.9 km, which is smaller than the eddy reference radius  $R_{max}$ . Since  $R_{max} > R_d$ , we  
 383 can objectively classify the eddy as a mesoscale structure. Since the local Rossby number  
 384 is not small, its dynamics can not be approximated by quasi-geostrophic theory.

385 We can compare our results with the data gathered during the experiment Latex08 in  
 386 the same area [*Hu et al.*, 2011a] conducted from September 1 to 5, 2008. Although the  
 387 generation process is different, these two coastal anticyclonic eddies have similar charac-  
 388 teristics in terms of position, extension and dynamical characteristics. This fact shows  
 389 the important influence of coast and bathymetry on the physical characteristics of these  
 390 mesoscale eddies.

391 *Hu et al.* [2011a] emphasized that the 2008 eddy interacts with the Northern Current  
 392 at the end of the Latex08 campaign, leading to its deformation and maybe to its death.  
 393 In our case, the presence and role of the Northern Current is much clearer (Figures 2b,c).  
 394 The NC has first created the eddy and then it affected it, reinforcing the current at its  
 395 southeastern part. This intensification could explain the asymmetric shape of the eddy.

396 Regarding the possible mechanisms for the formation of these anticyclonic eddies in the  
 397 literature, a few processes of generation have been listed in the introduction. The numer-  
 398 ical study of eddy generation in the western part of the GoL by *Hu et al.* [2011b] shows  
 399 that these eddies need two conditions to be generated: a persistent and strong northwest  
 400 wind and a strong stratification. This mechanism of generation has been identified in our  
 401 analysis. Indeed, the process of generation of the first modeled anticyclonic eddy *A1* cor-

402 responds to *Hu et al.* [2011b]’s process with the two conditions described above. A strong  
403 northwesterly wind is observed from June 19 to 21 and an intermediate stratification is  
404 noted at the end of June with an absolute value of potential energy anomaly greater than  
405  $60 \text{ J m}^{-3}$ .

406 Instead, for anticyclonic eddy *A2-Latex09*, we propose a new process of generation, as-  
407 sociated with the NC. This new mechanism starts with the generation of an anticyclonic  
408 circulation extending over a large part of the coastal area (Figure 6e). The generation of  
409 this anticyclonic circulation, precursor to the eddy, is not analyzed in this study but it  
410 could have been generated by the mechanism proposed by *Hu et al.* [2011b]. Interaction  
411 with a meander of the Northern Current and the presence of the coast induces the latitu-  
412 dinal separation of this anticyclonic circulation into two eddies, the northern one in the  
413 GoL and the southern one on the Catalan shelf. To our knowledge, this generation process  
414 has not been proposed before. Indeed the combined analysis of *Rubio et al.* [2005, 2009a]  
415 suggests that Catalan eddies are generated downstream of Cape Creus as a result of a  
416 flow separation triggered by an intense northwest wind event in the GoL. While *Garreau*  
417 *et al.* [2011] indicate that GoL eddies flow southward creating Catalan eddies after a burst  
418 of southeasterlies and northerlies. The authors conclude that the death of GoL eddies is  
419 clearly linked to the birth of strong Catalan eddies. In our case, the detachment of a part  
420 of the eddy does not lead to the death of *A2-Latex09*. The formation of this transient  
421 structure comes from the encounter of the *A2-Latex09* with Cape Creus. The generation  
422 of this transient structure causes a loss of mass and vorticity for *A2-Latex09*. In the *in-situ*  
423 measurements, a small structure is detected in the same spatial area and at the same time  
424 (Figure 8b) as the one given by the model (Figure 8a). When drifter No. 83632 starts

425 to loop outside the eddy (Figure 8b), drifting toward the south, its rotation period (39  
426 hours) eliminates the occurrence of an inertial oscillation. After  $\sim 6$  days this drifter is  
427 caught by the *Catalan Eddy* located at  $3^{\circ}11'E-41^{\circ}35'N$ . The generation of the transient  
428 structure moving from *A2-Latex09* toward the *Catalan Eddy* in the model results can  
429 explain the trajectories of these drifters. From the *in-situ* experiment it is clear that the  
430 generation of this structure leads directly to a transfer of mass from the eddy of the GoL  
431 to the eddy of the Catalan shelf.

432 This study gives a more complete and consistent picture of the GoL coastal eddy dy-  
433 namics. A full 3D analysis from numerical simulation will be made with the objective  
434 of better understanding the remaining open questions about the generation of the an-  
435 ticyclonic circulation, first step of the proposed new generation process. Besides, this  
436 numerical modeling work would be useful to explore the coupled physical and biogeo-  
437 chemical dynamics at mesoscale and the role of mesoscale eddies in the transfers between  
438 the GoL coastal zone and the neighboring coastal regions.

439 **Acknowledgments.** The LATEX project is supported by the programs LEFE/IDAO  
440 and LEFE/CYBER of the INSU-Institut National des Sciences de l'Univers and by the  
441 Region PACA-Provence Alpes Côte d'Azur. The meteorological data were kindly supplied  
442 by Météo-France. We acknowledge the MFS program for OGCM outputs. We are warmly  
443 grateful to the crews of the R/V *Téthys II* for their assistance. We thank Z. Y. Hu for  
444 providing the last configuration of the model. The authors want to thank J. Bouffard and  
445 C. Yohia for precious comments and useful discussions. Marion Kersalé is financed by a  
446 MENRT Ph.D. grant.

## References

- 447 Albérola, C., C. Millot, and J. Font (1995), On the seasonal and mesoscale variabilities of  
448 the Northern Current during the PRIMO-0 experiment in the western Mediterranean  
449 Sea, *Oceanol. Acta*, *18*(2), 163–192.
- 450 Allou, A., P. Forget, and J. L. Devenon (2010), Submesoscale vortex structures at the  
451 entrance of the Gulf of Lions in the Northwestern Mediterranean Sea, *Cont. Shelf Res.*,  
452 *30*, 724–732, doi:10.1016/j.csr.2010.01.006.
- 453 Burchard, H., and R. Burchard (2008), A dynamic equation for the potential energy  
454 anomaly for analysing mixing and stratification in estuaries and coastal seas, *Estuarine,  
455 Coastal Shelf Science*, *77*(4), 679–687, doi:10.1016/j.ecss.2007.10.025.
- 456 Casella, E., A. Molcard, and A. Provenzale (2011), Mesoscale vortices in the Ligurian  
457 Sea and their effect on coastal upwelling processes, *J. Mar. Sys.*, *88*(1), 12–19, doi:  
458 10.1016/j.jmarsys.2011.02.019.
- 459 Conan, P., and C. Millot (1995), Variability of the Northern Current off Marseilles, western  
460 Mediterranean Sea, from February to June 1992, *Oceanol. Acta*, *18*(2), 193–205.
- 461 Crawford, W. R. (2002), Physical characteristics of Haida Eddies, *Journal of Oceanogra-  
462 phy*, *58*(5), 703–713, doi:10.1023/A:1022898424333.
- 463 Crawford, W. R., and F. A. Whitney (1999), Mesoscale eddy swirl with data in Gulf of  
464 Alaska Ocean, *Eos, Trans. AGU*, *80*(33), 365–670.
- 465 Crawford, W. R., P. J. Brickley, and A. C. Thomas (2007), Mesoscale eddies dominate  
466 surface phytoplankton in northern Gulf of Alaska, *Prog. Oceanogr.*, *75*, 287–303, doi:  
467 10.1016/j.pocean.2007.08.016.

- 468 De Boer, G. J., J. D. Pietrzak, and J. C. Winterwerp (2008), Using the potential energy  
469 anomaly equation to investigate tidal straining and advection of stratification in a region  
470 of freshwater influence, *Ocean Model.*, *22*, 1–11.
- 471 Dencausse, G. J., M. Arhan, and S. Speich (2010), Routes of agulhas rings in the south  
472 eastern cape basin, *Deep-Sea Res. I*, *57*, 1406–1421, doi:10.1016/j.dsr.2010.07.008.
- 473 Denman, K. L., and H. J. Freeland (1985), Correlation scales, objective mapping and a  
474 statistical test of geostrophy over the continental shelf, *J. Mar. Res.*, *43*(3), 517–539,  
475 doi:10.1357/002224085788440402.
- 476 Di Lorenzo, E., M. G. G. Foreman, and W. R. Crawford (2005), Modelling the generation  
477 of Haida Eddies, *Deep-Sea Res. II*, *52*, 853–873, doi:10.1016/j.dsr2.2005.02.007.
- 478 Doglioli, A. M., A. Griffa, and M. G. Magaldi (2004), Numerical study of a coastal current  
479 on a steep slope in presence of a cape: The case of the Promontorio di Portofino,  
480 *J. Geophys. Res.*, *109*, C12033, doi:10.1029/2004JC002422.
- 481 Doglioli, A. M., B. Blanke, S. Speich, and G. Lapeyre (2007), Tracking coherent structures  
482 in a regional ocean model with wavelet analysis: application to Cape Basin Eddies,  
483 *J. Geophys. Res.*, *112*, C05043, doi:10.1029/2006JC003952.
- 484 Eide, L. I. (1979), Evidence of a topographically trapped vortex on the Norwegian conti-  
485 nental shelf, *Deep-Sea Res. I*, *26*(6), 601–621, doi:10.1016/0198-0149(79)90036-0.
- 486 Estournel, C., X. Durrieu de Madron, P. Marsaleix, F. Auclair, C. Julliand, and R. Ve-  
487 hil (2003), Observation and modeling of the winter coastal oceanic circulation in the  
488 Gulf of Lion under wind conditions influenced by the continental orography (FETCH  
489 experiment), *J. Geophys. Res.*, *108*(C3), 8059, doi:10.1029/2001JC000825.

- 490 Flexas, M. M., X. Durrieu de Madron, M. A. Garcia, M. Canals, and P. Arnau (2002),  
491 Flow variability in the Gulf of Lions during the MATER HFF experiment (March-May  
492 1997), *J. Mar. Sys.*, *33-34*, 197–214, doi:DOI: 10.1016/S0924-7963(02)00059-3.
- 493 Foreman, M. G. G., W. Callendar, A. MacFadyen, B. M. Hickey, R. E. Thomson, and  
494 E. Di Lorenzo (2008), Modeling the generation of the juan de fuca eddy, *J. Geo-*  
495 *phys. Res.*, *113*(C03006), doi:10.1029/2006JC004082.
- 496 Fratantoni, D. M., W. E. Johns, and T. L. Townsend (1995), Rings of the North Brazil  
497 Currents: their structure and behavior inferred from observations and a numerical sim-  
498 ulation, *J. Geophys. Res.*, *100*(C6), 10.633–10.654, doi:10.1029/95JC00925.
- 499 Freeland, H. J., and K. L. Denman (1982), A topographically controlled upwelling center  
500 off southern Vancouver Island, *J. Mar. Sys.*, *40*(4), 1069–1093.
- 501 Freeland, H. J., and P. McIntosh (1989), The vorticity balance on the southern British  
502 Columbia continental shelf, *Atmos.-Ocean*, *27*(4), 643–657.
- 503 Garreau, P., V. Garnier, and A. Schaeffer (2011), Eddy resolving modelling of the Gulf of  
504 Lions and Catalan Sea, *Ocean Dynam.*, *61*, 991–1003, doi:10.007/s10236-011-0399-2.
- 505 Hamilton, P., G. S. Fargion, and D. C. Biggs (1999), Loop Current eddy paths in  
506 the western Gulf of Mexico, *J. Phys. Oceanogr.*, *29*(6), 1180–1207, doi:10.1175/1520-  
507 0485(1999)029;1180:LCEPIT;2.0.CO;2.
- 508 Hu, Z. Y., A. A. Doglioli, A. M. Petrenko, P. Marsaleix, and I. Dekeyser (2009), Nu-  
509 merical simulations of eddies in the Gulf of Lion, *Ocean Model.*, *28*(4), 203 – 208,  
510 doi:10.1016/j.ocemod.2009.02.004.
- 511 Hu, Z. Y., A. A. Petrenko, A. M. Doglioli, and I. Dekeyser (2011a), Study of mesoscale  
512 anticyclonic eddy in the western part of the Gulf of Lion, *J. Mar. Sys.*, *88*, 3–11, doi:

- 513 10.1016/j.jmarsys.2011.02.008.
- 514 Hu, Z. Y., A. A. Petrenko, A. M. Doglioli, and I. Dekeyser (2011b), Numerical study of  
515 eddy generation in the western part of the Gulf of Lion, *J. Geophys. Res.*, *116*, C12030,  
516 doi:10.1029/2011JC007074.
- 517 Kirwan Jr., A. D., J. K. Lewis, A. W. Indest, P. Reinersman, and I. Quintero (1988),  
518 Observed and Simulated Kinematic Properties of Loop Current Rings, *J. Geophys. Res.*,  
519 *93*(C2), 1189–1198, doi:10.1029/JC093iC02p01189.
- 520 Ladd, C. M., N. B. Kachel, C. W. Mordy, and P. J. Stabeno (2005), Observations from  
521 a Yakutat eddy in the northern Gulf of Alaska, *J. Geophys. Res.*, *110*(C03003), doi:  
522 10.1029/2004JC002710.
- 523 Lathuilière, C., V. Echevin, M. Lévy, and G. Madec (2010), On the role of the mesoscale  
524 circulation on an idealized coastal upwelling ecosystem, *J. Geophys. Res.*, *115*, C09018,  
525 doi:10.1029/2009JC005827.
- 526 Lewis, J. K., and A. D. Kirwan Jr. (1985), Some observations of ring topography and  
527 ring-ring interactions in the Gulf of Mexico, *J. Geophys. Res.*, *90*(C5), 9017–9028, doi:  
528 10.1029/JC090iC05p09017.
- 529 MacFadyen, A., and B. M. Hickey (2010), Generation and evolution of a topographically  
530 linked, mesoscale eddy under steady and variable wind-forcing, *Cont. Shelf Res.*, *30*(13),  
531 1387–1402, doi:10.1016/j.csr.2010.04.001.
- 532 MacFadyen, A., B. M. Hickey, and W. P. Cochlan (2008), Influences of the Juan de Fuca  
533 Eddy on circulation, nutrients, and phytoplankton production in the northern California  
534 Current System, *J. Geophys. Res.*, *113*(C08008), doi:10.1029/2007JC004412.

- 535 Magaldi, M., T. Özgökmen, A. Griffa, and M. Rixen (2010), On the response of a turbulent  
536 coastal buoyant current to wind events: the case of the Western Adriatic Current,  
537 *Ocean Dynam.*, *60*, 93–122, doi:10.1007/s10236-009-0247-9.
- 538 Marsaleix, P., F. Auclair, and C. Estournel (2006), Considerations on Open Boundary  
539 Conditions for Regional and Coastal Ocean Models, *J. Atmos. Ocean. Technol.*, *23*,  
540 1604–1613, doi:10.1175/JTECH1930.1.
- 541 Marsaleix, P., F. Auclair, J. Floor, M. Herrmann, C. Estournel, I. Pairaud, and C. Ulses  
542 (2008), Energy conservation issues in sigma-coordinate free-surface ocean models,  
543 *Ocean Model.*, *20*, 61–89, doi:10.1016/j.ocemod.2007.07.005.
- 544 Melson, A., S. D. Meyers, H. E. Hurlburt, E. J. Metzger, and J. J. O’Brien (1999), ENSO  
545 effects on Gulf of Alaska eddies, *Earth Interactions* *3*, 003, doi:10.1175/1087-3562.
- 546 Millot, C. (1979), Wind induced upwellings in the Gulf of Lions, *Oceanol. Acta*, *2*, 261–  
547 274.
- 548 Millot, C. (1982), *Analysis of upwelling in the Gulf of Lions - Hydrodynamics of semi-*  
549 *enclosed seas: Proceedings of the 13th International Liège Colloquium on Ocean Hydro-*  
550 *dynamics.*, vol. 34, 143-153 pp., Elsevier Oceanogr. Ser., Amsterdam, The Netherlands.
- 551 Millot, C. (1990), The Gulf of Lions’ hydrodynamics, *Cont. Shelf Res.*, *10*, 885–894, doi:  
552 10.1016/0278-4343(90)90065-T.
- 553 Mitchelson-Jacob, G., and S. Sundby (2001), Eddies of Vestfjorden, Norway,  
554 *Cont. Shelf Res.*, *21*(16-17), 1901–1918, doi:10.1016/S0278-4343(01)00030-9.
- 555 Nencioli, F., V. S. Kuwahara, T. D. Dickey, Y. M. Rii, and R. R. Bidigare (2008), Physical  
556 dynamics and biological implications of a mesoscale eddy in the lee of Hawai’i : Cyclone  
557 Opal observations during E-FLUX III, *Deep-Sea Res. II*, *55*(10-13), 1252–1274, doi:

558 10.1016/j.dsr2.2008.02.003.

559 Nencioli, F., F. d'Ovidio, A. M. Doglioli, and A. A. Petrenko (2011), Surface coastal  
560 circulation patterns by in-situ detection of Lagrangian coherent structures, *Geo-*  
561 *phys. Res. Lett.*, *38*(L17604), doi:10.1029/2011GL048815.

562 Petrenko, A. A. (2003), Variability of circulation features in the Gulf of Lion NW Mediter-  
563 ranean Sea. Importance of inertial currents, *Oceanol. Acta*, *26*, 323–338.

564 Petrenko, A. A., Y. Leredde, and P. Marsaleix (2005), Circulation in a stratified  
565 and wind-forced Gulf of Lions, NW Mediterranean Sea: in situ and modeling data,  
566 *Cont. Shelf Res.*, *25*, 7–27, doi:10.1016/j.csr.2004.09.004.

567 Pinardi, N. (2003), The Mediterranean ocean forecasting system : first phase of implemen-  
568 tation (1998-2001), *Ann. Geophys.*, *21*, 3–20, doi:10.5194/angeo-21-3-2003.

569 Richardson, P. L., G. E. Hufford, and R. I. Limeburner (1994), North Brazil Current  
570 retroflection eddies, *J. Geophys. Res.*, *99*(C3), 5081–5093, doi:doi:10.1029/93JC03486.

571 Rubio, A., P. Arnau, M. Espino, M. Flexas, G. Jordà, J. Salat, J. Puigdefàbregas, and  
572 A. S.-Arcilla (2005), A field study of the behaviour of an anticyclonic eddy on the  
573 Catalan continental shelf (NW Mediterranean), *Prog. Oceanogr.*, *66*(2-4), 142–156, doi:  
574 10.1016/j.pocean.2004.07.012.

575 Rubio, A., B. Barnier, G. Jordà, M. Espino, and P. Marsaleix (2009a), Origin and dy-  
576 namics of mesoscale eddies in the Catalan Sea (NW Mediterranean): Insight from a nu-  
577 merical model study, *J. Geophys. Res.*, *114*(C06009), 1–17, doi:10.1029/2007JC004245.

578 Rubio, A., B. Blanke, S. Speich, N. Grima, and C. Roy (2009b), Mesoscale eddy activity  
579 in the southern Benguela upwelling system from satellite altimetry and model data,  
580 *Prog. Oceanogr.*, *83*(1-4), 288–295, doi:10.1016/j.pocean.2009.07.029.

- 581 Saetre, R. (1999), Features of the central Norwegian shelf, *Cont. Shelf Res.*, *19*(14), 1809–  
582 1831, doi:10.1016/S0278-4343(99)00041-2.
- 583 Sammari, C., C. Millot, and L. Prieur (1995), Aspects of the seasonal and mesoscale vari-  
584 abilities of the Northern Current inferred from the PROLIG-2 and PROS-6 experiments,  
585 *Deep-Sea Res. I*, *42*(6), 893–917, doi:10.1016/0967-0637(95)00031-Z.
- 586 Schaeffer, A., A. Molcard, P. Forget, P. Fraunié, and P. Garreau (2011), Generation  
587 mechanisms for mesoscale eddies in the Gulf of Lions : radar observation and modeling,  
588 *Ocean Dynam.*, *61*, 1587–1609, doi:10.1007/s10236-011-0482-8.
- 589 Siegel, D. A., P. Peterson, D. J. McGillicuddy, S. Maritorena, and N. B. Nelson  
590 (2011), Biooptical footprints created by mesoscale eddies in the Sargasso Sea, *Geo-*  
591 *phys. Res. Lett.*, *38*(L13608), doi:doi:10.1029/2011GL047660.
- 592 Signell, R. P., and W. R. Geyer (1991), Transient eddy Formation Around Headlands, *J.*  
593 *Geophys. Res.*, *96*(C2), 2561–2575, doi:10.1029/90JC02029.
- 594 Souza, J. M. A. C., C. de Boyer Montégut, and P. Y. Le Traon (2011), Comparison between  
595 three implementations of automatic identification algorithms for the quantification and  
596 characterization of mesoscale eddies in the South Atlantic Ocean, *Ocean Sc.*, *7*, 317–334,  
597 doi:10.5194/os-7-317-2011.
- 598 Tabata, S. (1982), The anticyclonic baroclinic eddy off Sitka, Alaska, in the  
599 northeast Pacific Ocean, *J. Phys. Oceanogr.*, *12*, 1260–1282, doi:10.1175/1520-  
600 0485(1982)012<1260:TABEOS>2.0.CO;2.
- 601 Tully, J. (1942), Surface non-tidal currents in the approaches to Juan de Fuca Strait, *J.*  
602 *Fish. Res. Board Can.*, *5b*(4), 398–409, doi:10.1139/f40-041.

603 Vidal, V. M. V., F. V. Vidal, and J. M. Perez-Molero (1992), Collision of a Loop Current  
 604 anticyclonic ring against the continental slope of the western Gulf of Mexico, *J. Geo-*  
 605 *phys. Res.*, *97*(C2), 2155–2172, doi:10.1029/91JC00486.

606 Vukovich, F. M., and E. Waddel (1991), Interaction of a warm ring with the western slope  
 607 in the Gulf of Mexico, *J. Phys. Oceanogr.*, *21*(7), 1062–1074.

**Table 1.** Start and end dates of the transects.

Transect	Start		End	
	Day	Hour (GMT)	Day	Hour (GMT)
1	Aug. 25	01h38	Aug. 25	04h48
2	Aug. 25	18h27	Aug. 25	23h39
3	Aug. 26	21h24	Aug. 27	01h16
4	Aug. 27	21h31	Aug. 28	03h54

**Table 2.** Summary of the calculation of the position of the center of the eddy for each transect.

The along transect diameter at the depth given in column 2 is provided in column 3.

Transect	Depth (m)	Diameter (km)	Single-depth transect center	Depth-averaged transect center	Transect-averaged eddy center
1	-11	30	<i>C1_11</i> : 3°33'E - 42°33'N	C1: 3°34'E - 42°33'N	C: 3°34'E - 42°33'N
	-15	33	<i>C1_15</i> : 3°33'E - 42°33'N		
	-19	35	<i>C1_19</i> : 3°35'E - 42°33'N		
2	-11	30	<i>C2_11</i> : 3°35'E - 42°30'N	C2: 3°34'E - 42°31'N	
	-15	29	<i>C2_15</i> : 3°33'E - 42°31'N		
	-19	28	<i>C2_19</i> : 3°33'E - 42°32'N		
3	-11	24	<i>C3_11</i> : 3°35'E - 42°30'N	C3: 3°36'E - 42°32'N	
	-15	24	<i>C3_15</i> : 3°35'E - 42°33'N		
	-19	26	<i>C3_19</i> : 3°36'E - 42°34'N		
4	-11	24	<i>C4_11</i> : 3°33'E - 42°33'N	C4: 3°35'E - 42°34'N	
	-15	22	<i>C4_15</i> : 3°34'E - 42°34'N		
	-19	16	<i>C4_19</i> : 3°37'E - 42°34'N		

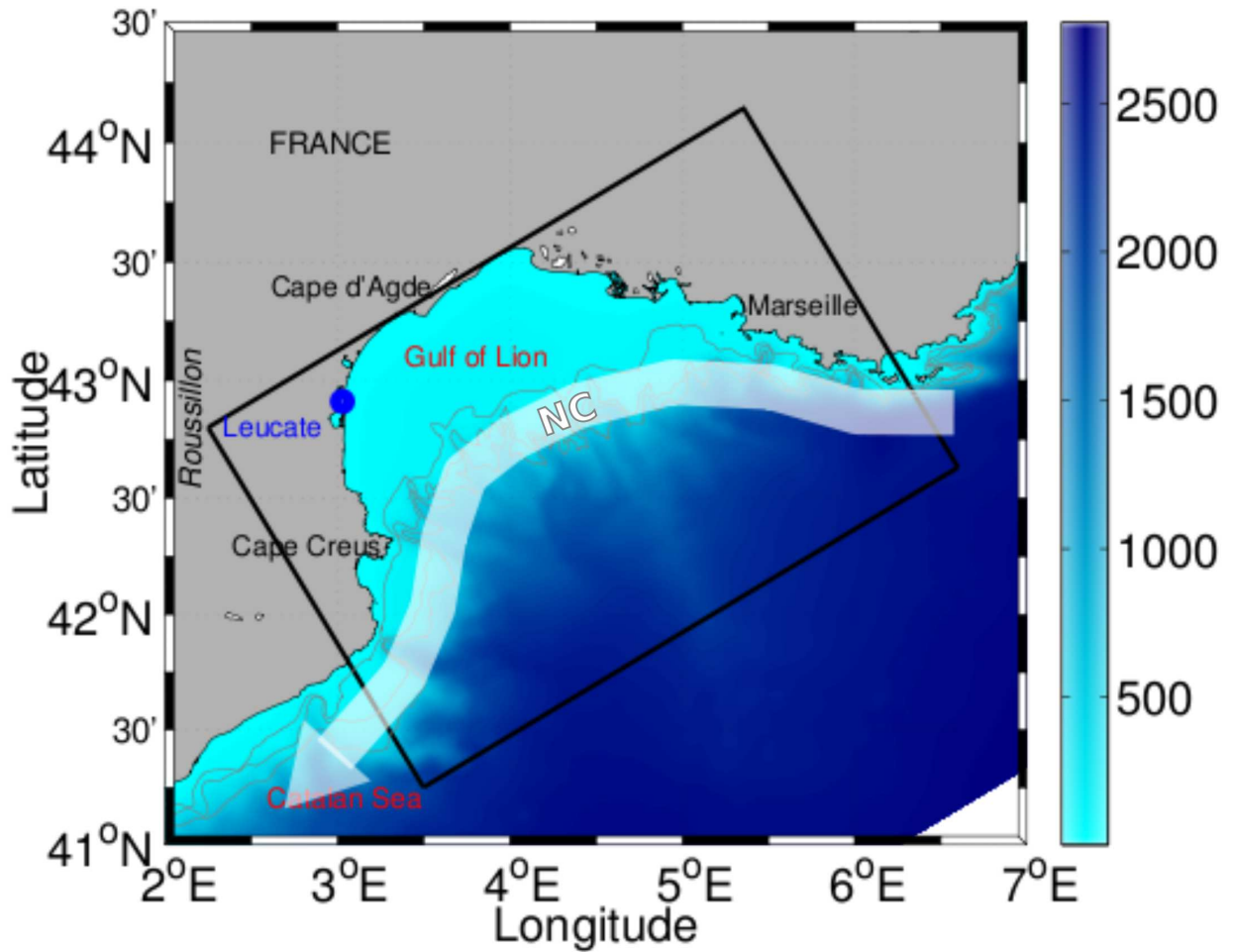


**Figure 1.** Model domain. The rectangle represents the model domain of  $1 \text{ km} \times 1 \text{ km}$  resolution. Shaded color represents the bathymetry [m]. Isobaths at 100, 200 and 500 m are plotted with thin lines. The white arrow shows the mean position of the Northern Current (NC).

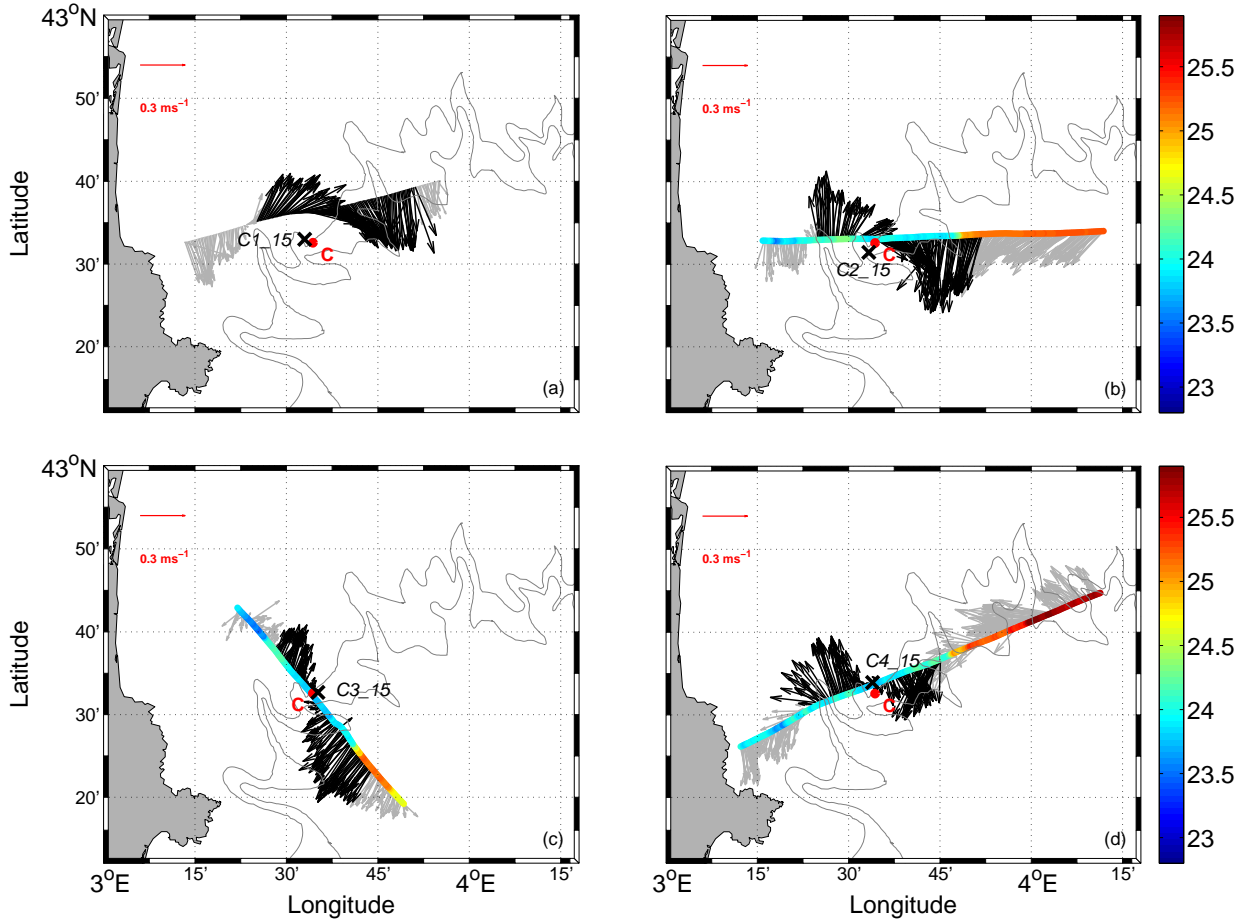


**Figure 2.** ADCP current vectors at 15m depth for Transect 1 (a), Transect 2 (b), Transect 3 (c) and Transect 4 (d). The colors on the transect represent the surface temperature data ( $^{\circ}\text{C}$ ) acquired along the trajectory. For each transect, the single-depth transect center at 15 m depth (black cross) is defined as the point for which the mean tangential velocity computed from the velocity vectors in black is maximum. The red dot corresponds to the eddy center.

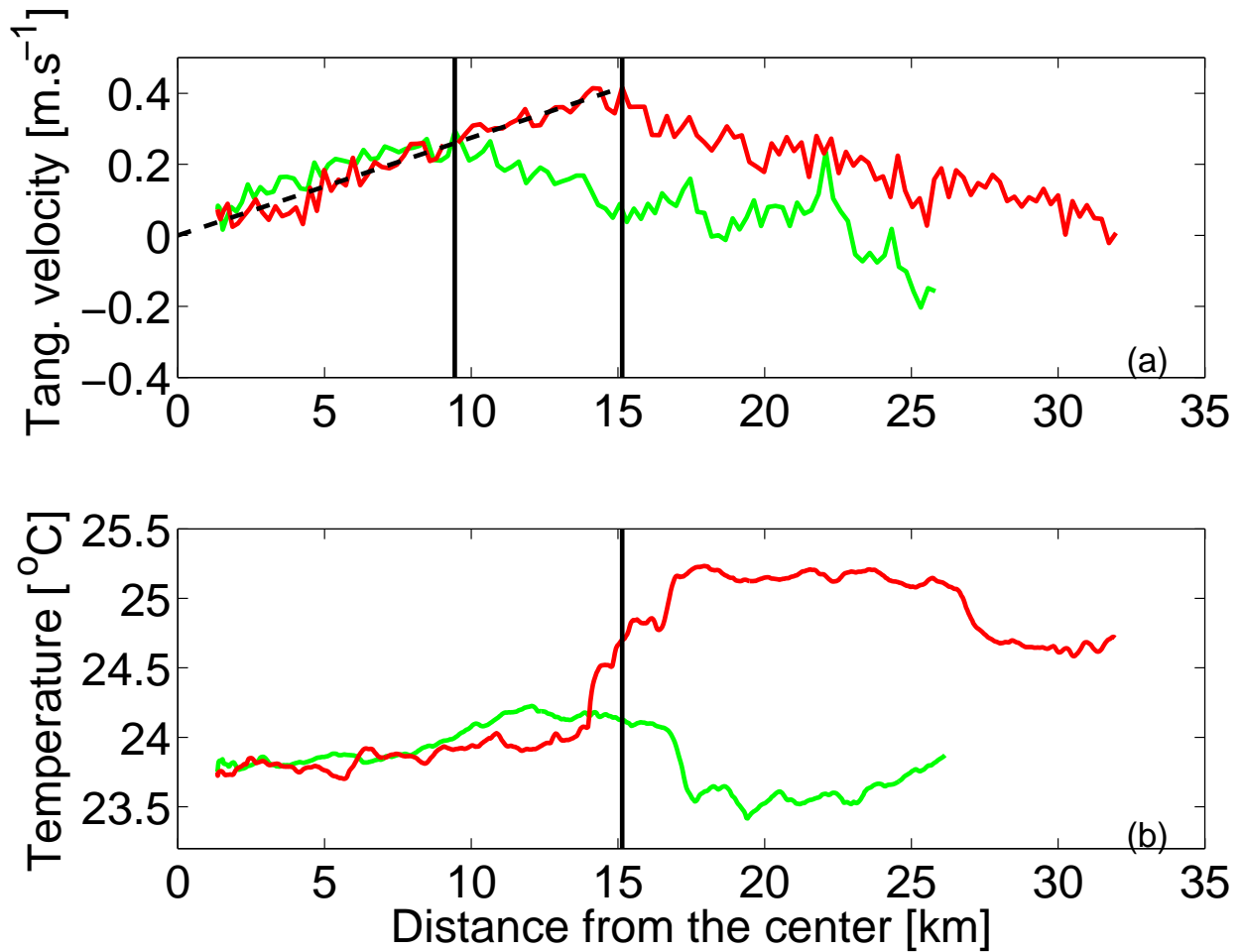


**Figure 3.** Distribution of tangential velocities at 15 m depth (a) and temperature at the surface (b) with respect to radial distance from *C3\_15*. The green line corresponds to the data collected before crossing the center (hence northwest of the center *C3\_15* for Transect 3) and the red line corresponds to the data collected after the center (southeast of it). Black lines represent the distance from *C3\_15* where the maximum values of tangential velocities are reached. The black dashed line shows the linear increase of the tangential velocities in the case of a theoretical solid body rotation.

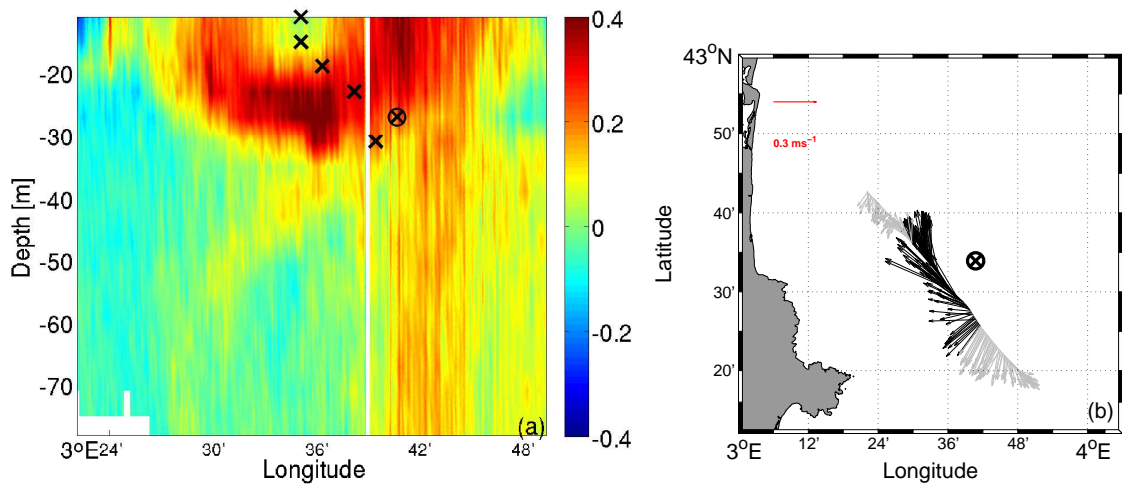


**Figure 4.** (a) Vertical section (depth versus longitude) of the tangential component (clockwise, positive) of the horizontal currents [ $\text{m s}^{-1}$ ] for Transect 3. White pixels represent no data. ADCP current vectors at 27 m depth (b) for Transect 3. The black cross represent the single-depth transect center. The black circle represents the single-depth transect center at 27 m depth, common to figures a and b.

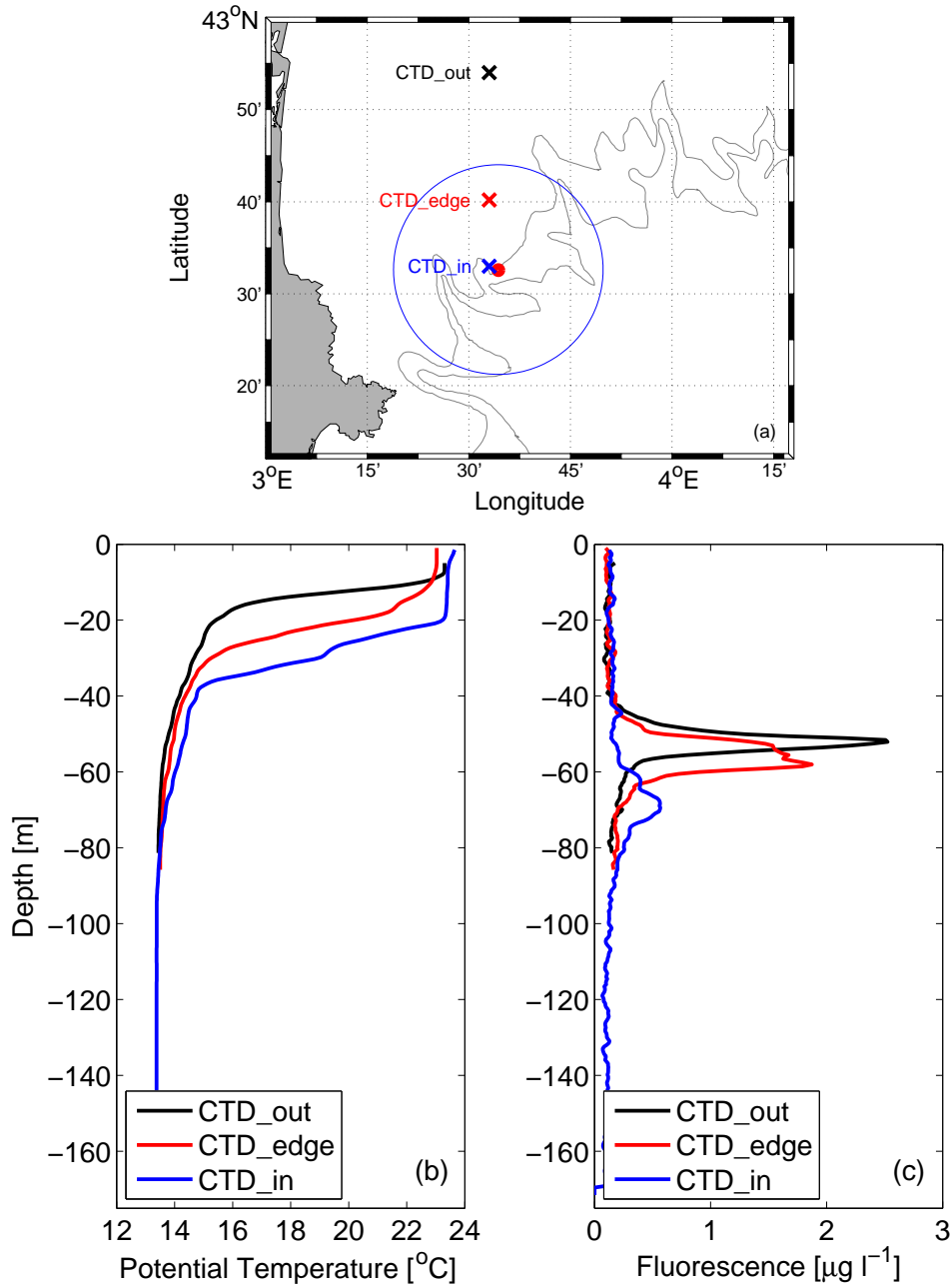


**Figure 5.** (a) The three crosses represent the positions of the CTD stations (CTD\_in, CTD\_edge, CTD\_out). The blue circle is centered at the eddy center **C** (red dot) with a radius equal to the one estimated for the eddy. Vertical profiles of potential temperature (b) and fluorescence (c) at three CTD stations on August 26 (CTD\_out: Outside part of the eddy located to the north; CTD\_edge: Northern edge of the eddy; CTD\_in: Inside part of the eddy).

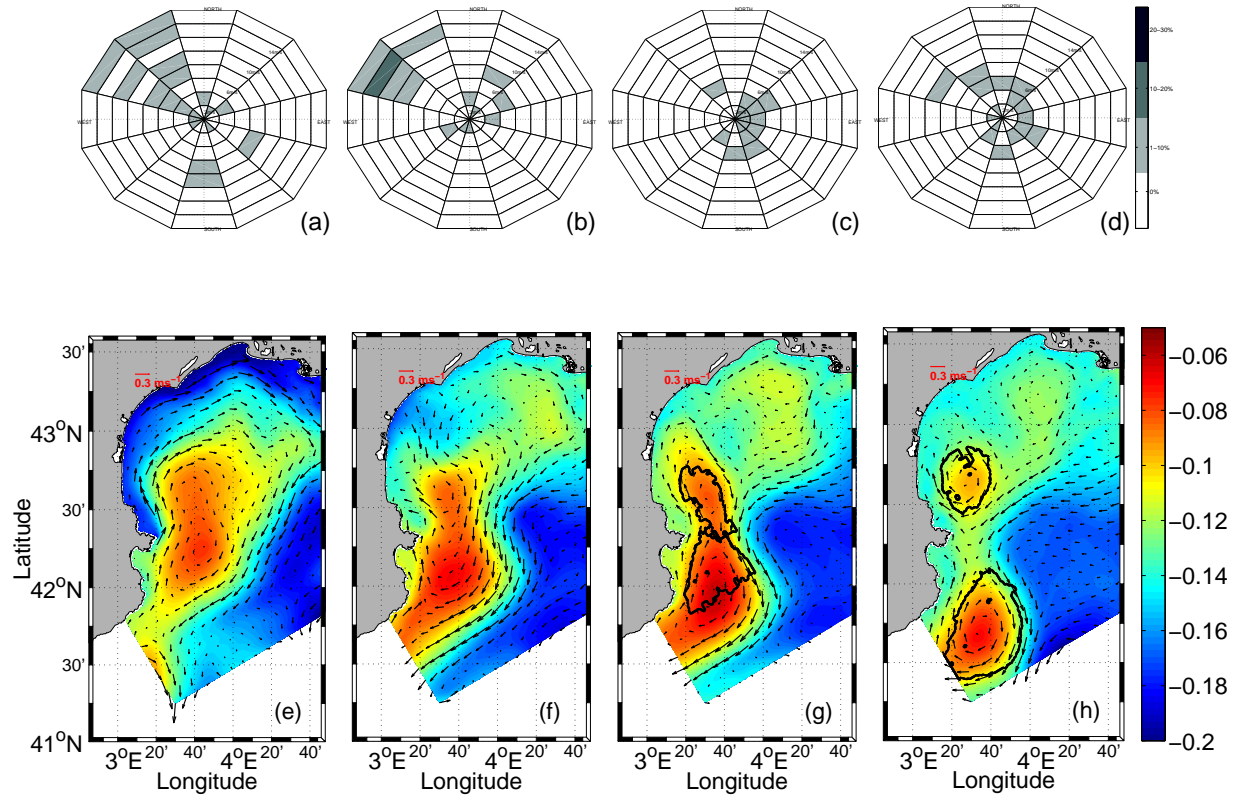


**Figure 6.** Time sequence of the generation process of *A2-Latex09* in 2009. Top: wind rose representation (intensity and frequency) at station Leucate on (a) 2009/07/18 to 20; (b) 2009/08/06 to 08; (c) 2009/08/14 to 16; (d) 2009/08/25 to 27; colors representing wind frequency (%). Bottom: sea surface height [m] and current velocity field at 5 m depth on (e) 2009/07/20; (f) 2009/08/08; (g) 2009/08/16; (h) 2009/08/27. Black contours in (g) and (h) show the eddies identification issued from the wavelet analysis.

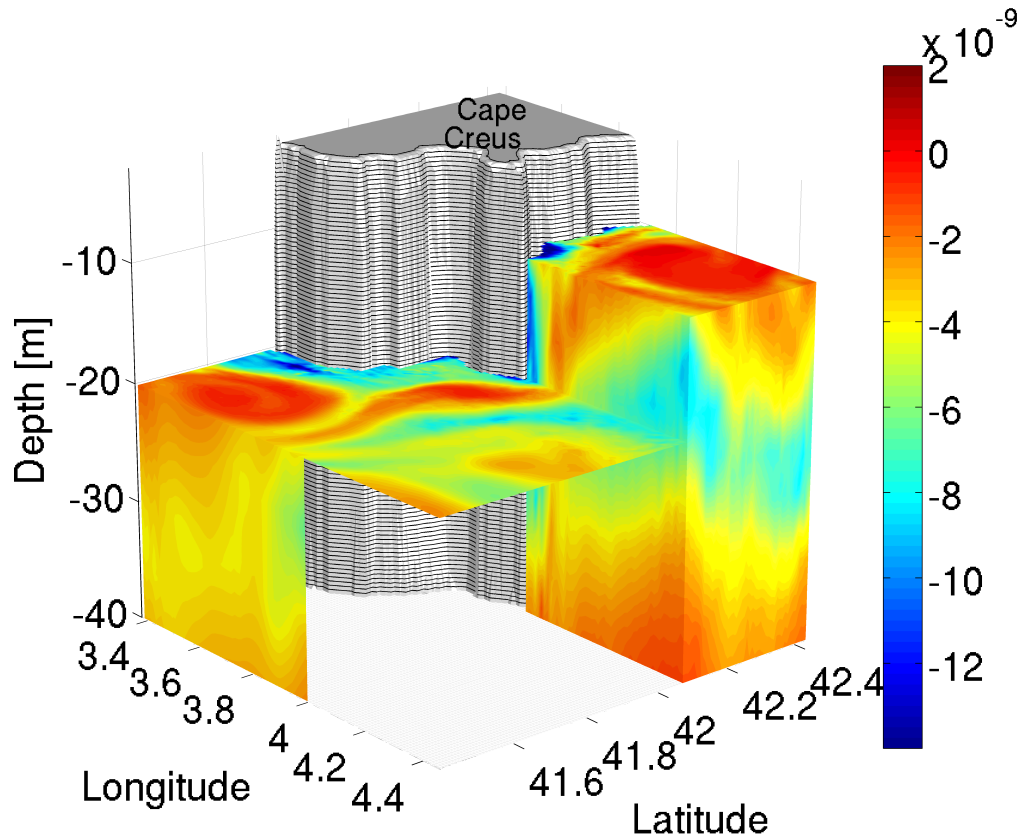


**Figure 7.** 3-dimensional sections of potential vorticity [ $\text{kg m}^{-4} \text{s}^{-1}$ ] in color on September 3. The coast is represented in gray with the position of the Cape Creus. At 10 m depth, in the first section, we can distinguish the presence of A2-Latex09 upstream the Cape Creus. In the lee of the Cape, the transient structure is evidenced at 20 m depth. The Catalan eddy is also visualized farther off the coast and until 40 m depth.

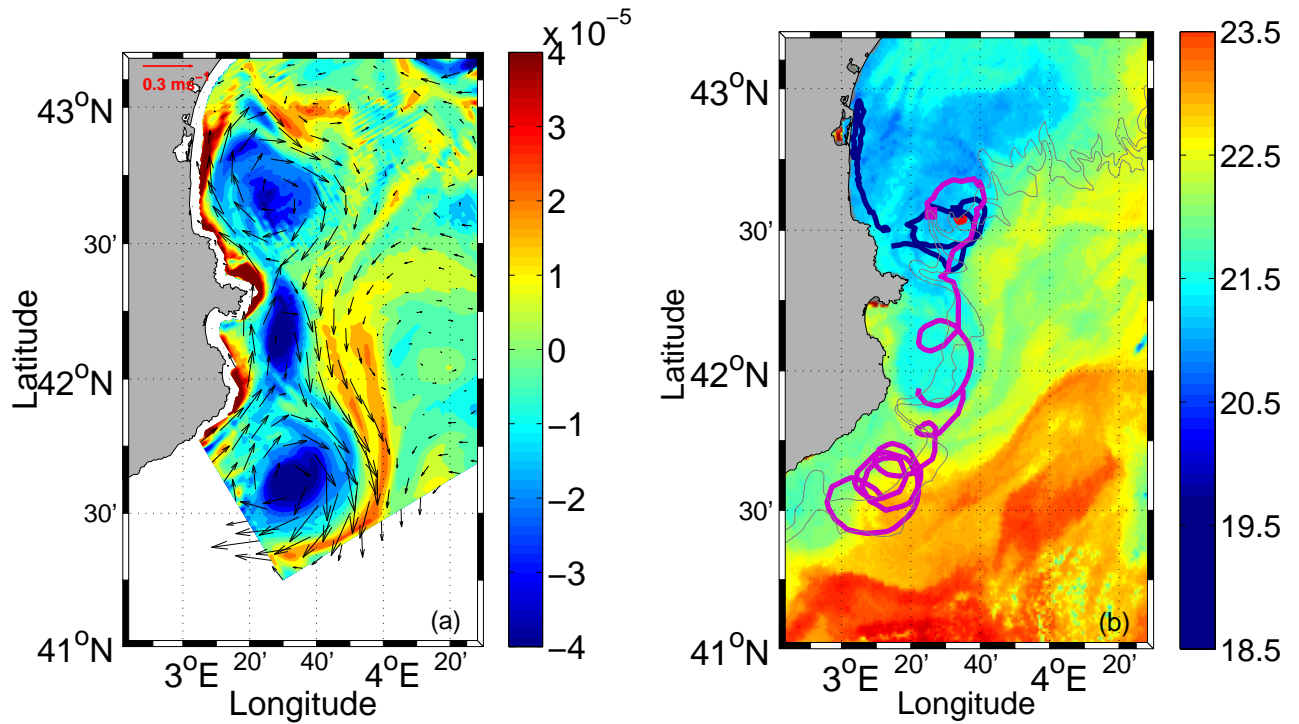


**Figure 8.** (a) Modeled relative vorticity [ $\text{s}^{-1}$ ] and current velocity field at 20 m depth on September 3. (b)  $SST_b$  satellite image on August 28 (data from Météo-France) and drifter trajectories (drifter No. 83631 in blue - drifter No. 83632 in purple) from August 26 to September 12. The squares represent the drifters' initial positions. The red dot corresponds to the eddy center.